

NON-UNIFORM PATCH LUMINANCE FOR GLOBAL ILLUMINATION

Buming Bian
University of Texas System — CHPC
Balcones Research Center
Commons Building, 1.154
Austin, TX 78712

Norman Wittels
Department of Civil Engineering Worcester Polytechnic Institute
Worcester, MA 01609

Donald S. Fussell
Department of Computer Science
University of Texas at Austin
Austin Texas 78712

ABSTRACT

A new radiosity model is presented in which all patches are represented as isoparametric elements and the patch luminances change bilinearly. The surfaces are tessellated into planar quadrilaterals and continuous surface luminance is maintained where patches meet. A new form factor, accounting for the luminance contributions between patches, is derived and calculated using hemisphere projections and Gaussian quadrature. Images generated from the new approach were tested by pixel-level comparison with real images acquired by a calibrated imaging system, and compared with the images generated by the uniform patch luminance radiosity. The comparison results indicate that fewer bilinear patches are required to achieve comparable luminance accuracy.

CR Categories and Subject Descriptors: I.3.3 [Computer Graphics]: Picture/Image Generation; Display Algorithm; I.3.7 [Computer Graphics]: three-dimensional Graphics and Realism.

General Terms: Algorithms.

Additional Key Words and Phrase: radiosity, accurate image, non-uniform patch luminance, pixel level comparison, image registration.

1. INTRODUCTION

Radiosity methods for photo-realistic image generation have recently been the subject of intensive research interest in computer graphics. These methods involve the accurate determination of surface luminances before the pixel image is rendered. Since each diffuse surface receives light from and emits light to other surfaces visible to it, this interreflection problem can be modelled as a set of equations relating the luminance of each surface to the luminances of all other surfaces in the scene.

The interreflection problem is equivalent to the radiosity method as used in thermal engineering studies of radiative heat transfer[10]. Surface luminance is a function of the light from sources and the interreflected light from other diffuse surfaces. The key concepts are energy conservation (all light leaving a surface must be accounted for) and energy equilibrium (the total light out of any surface equals the total light in times the surface reflectivity). In the radiosity calculation, surfaces in a scene are divided into planar patches. The luminance at any point on a patch due to the light emitted by another patch can be calculated using the analytical methods summarized in [12, 14, 17]. The luminance can be expressed as:

$$L = \rho \int_{A_s} L_s \frac{\cos \theta_k \cos \theta_l}{\pi r^2} da_s \quad (1)$$

where ρ is the surface reflectance, L_s is the source luminance, r is the distance between the point and the source, θ_k is the angle between r and the normal of the point, θ_l is the angle between r and the normal of the source, and the da_s is the differential area on the source.

Current radiosity methods assume that the luminance is uniform on each patch[9]. Thus, if we use only average luminance values for each patch in a set of M patches, then L_k , the luminance of patch k , is a linear function of the luminances of the other patches, plus the self-illumination term L_k^0 :

$$L_k = \rho_k \sum_{l=1}^M F_{kl} L_l + L_k^0 \quad (2)$$

where ρ_k is the reflectance of patch k , and the form factor F_{kl} , given by

$$F_{kl} = \frac{1}{A_k} \int_{A_k} \int_{A_l} \frac{\cos \theta_k \cos \theta_l}{\pi r^2} da_l da_k$$

is a function of the relative positions and orientations of the two patches. A_k is the area of patch k , da_l and da_k are,



respectively, the differential area on patch l and k . For an enclosed scene, additional information can be obtained by using the following three principles. Energy conservation requires that the energy leaving a surface must equal the energy into that surface times the surface reflectivity. That is,

$$\sum_{l=1}^M \frac{A_k}{A_l} F_{kl} = 1 \quad (3)$$

for $k = 1, \dots, M$, where A_k is the area of patch k . Reciprocity (the Second Law of Thermodynamics) requires that:

$$A_k F_{kl} = A_l F_{lk}$$

and the principle that no planar polygon may illuminate itself can be written as:

$$F_{kk} = 0$$

A number of algorithms [1, 2, 5, 6, 7, 8, 13, 16] have been developed for computing form factors and for solving the interreflection problem. All assume patches of uniform intensity. This assumption simplifies the calculation of form factors, but it can in many cases require that a scene be subdivided into a number of patches.

In this paper we develop a new radiosity model which allows the luminance of surface patches to vary bilinearly across their patches. We develop an effective approach to calculate form factors for such patches by using hemispherical projections and Gaussian quadrature in situations when analytic solutions do not exist. We then undertake a systematic comparison of images produced with bilinear luminance patches and uniform luminance patches to determine the effectiveness of our model in increasing accuracy with a smaller number of patches. This is done by comparing these images against a calibrated real world test scene.

The paper is organized as follows. Section 2 presents our radiosity model and develops a form factor function from a bilinearly illuminated quadrilateral patch to a receiver vertex. Section 3 shows how to compute such form factors using hemispherical projection and Gaussian quadrature. Section 4 contains the experimental results of our accuracy tests.

2. NEW RADIOSITY APPROACH

The basic question addressed in this section is as follows: Given that a patch has non-uniform luminance, what mathematical model of that luminance will be sufficiently accurate, yet still allow for practical calculation of interreflection form factors? Any surface luminance distribution which is an analytic function $f(x, y)$ of the coordinates has a Taylor's series expansion:

$$f(x, y) = f(x_1, y_1) + f_x(x_1, y_1)(x - x_1) + f_y(x_1, y_1)(y - y_1) \\ + f_{xy}(x_1, y_1)(x - x_1)(y - y_1) + \dots$$

where $f(x_1, y_1)$, $f_x(x_1, y_1)$, and $f_y(x_1, y_1)$ are, respectively, the value and partial derivatives of the function at the point (x_1, y_1) and $f_{xy}(x_1, y_1)$ is the mixed second derivative. Standard radiosity approaches assume that the luminance is constant, therefore they use only the zero order term $f(x_1, y_1)$ to describe the surface luminance of a patch, that is, $f(x, y) = f(x_1, y_1)$ for a given polygonal patch. To model non-uniform luminances, at least the first order or linear terms need be used. A continuous luminance model and quadrilateral tessellation model based upon the crossterm Taylor series expansion is used in our discussion.

The interior luminance, in a quadrilateral patch, may be expressed as a bilinear interpolation of the luminances at the four vertices $L_j (j = 0, 1, 2, 3)$:

$$L = \sum_{j=0}^3 N_j L_j \quad (4)$$

where the N_j , called shape functions, depend only upon the shape of the quadrilateral. Their explicit forms are given as follows:

$$N_0 = \frac{1}{4}(1-s)(1-t) \quad N_1 = \frac{1}{4}(1+s)(1-t)$$

$$N_2 = \frac{1}{4}(1+s)(1+t) \quad N_3 = \frac{1}{4}(1-s)(1+t)$$

where s and t are parameters, satisfying $|s| \leq 1$, $|t| \leq 1$. Shape functions satisfy the following rules: 1) The mapping between the a plane in the xyz space and the st space is homeomorphic. 2) Each shape function has value one at its own vertex and zero at others. 3) Each shape function is zero along any edge that does not contain its vertex. 4) Each shape function is a polynomial of the same degree as the interpolation equation.

In the simulation, triangles and quadrilaterals were selected as primitives. It is easy to show that the triangle is basic; any planar polygon can be exactly decomposed into triangles. Since triangles are degenerated quadrilaterals with two vertices coinciding, all the patches will be represented as quadrilaterals.

Now consider the interreflection between two diffuse patches with luminance described by Eq.(1). From Eq.(4), the luminance contribution of patch l to the i th vertex of patch k , (see Fig.1), is:

$$L_i = \rho_k \int_{A_l} \sum_{j=0}^3 N_j L_j \frac{\cos \theta_i \cos \theta_j}{\pi r^2} da_l = \rho_k \sum_{j=0}^3 K_{ij} L_j$$

where ρ_k is the diffuse reflectivity of patch k , L_j is the luminance of the j th vertex of patch l , da_l is a differential area on patch l , and

$$K_{ij} = \int_{A_l} N_j \frac{\cos \theta_i \cos \theta_j}{\pi r^2} da_l \quad (5)$$



is the new form factor corresponding to the bilinear patch luminance distribution.

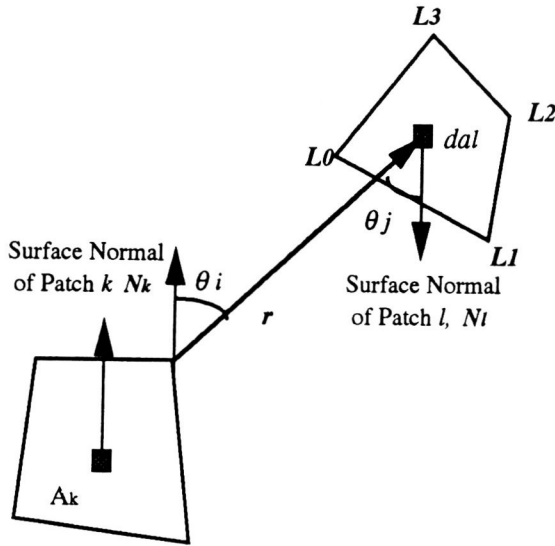


Fig.1 Luminance contribution from one patch to one vertex of another patch

Therefore, the total luminance from patch l to the vertex i of patch k is a linear combination of the vertex luminances of patch l , and vice versa. For an enclosed scene with M patches, there will be $4M$ vertices. With self-luminance included, the luminance on each vertex can be written as

$$L_i = \rho_k \sum_{j=1}^N K_{ij} L_j + L_i^0 \quad (6)$$

where $N \leq 4M$. $4M$ is an upper bound; the actual number may be lower. Many of the vertices coincide where patches meet and the redundancies can be eliminated. For a large surface subdivided into K^2 patches, there are only $(K + 1)^2$ independent vertices. In Eq.(6), i is the vertex index of patch k and j is the vertex index of patch l , with $k = (i \text{ mod } 4)$ and $l = (j \text{ mod } 4)$.

Before calculating the form factors, the physical correctness of the new model needs to be verified. That is, we need to see if this model follows the energy conservation and reciprocity laws. To maintain energy conservation, the energy leaving a surface must equal the energy arriving at this surface times the reflectivity. The luminance at a point on patch k equals the summation of all the contributions from the whole scene and the total flux into the patch is

$$\begin{aligned} \Phi_{in} &= \frac{\pi}{\rho_k} \int_{A_k} L_k da_k \\ &= \frac{\pi}{\rho_k} \int_{A_k} \sum_{i=0}^3 N_i L_i da_k \\ &= \frac{\pi}{\rho_k} \sum_{i=0}^3 L_i A_i \end{aligned}$$

From Eq.(6), the total flux out of the patch k is the summation of the luminances received by the rest of the patches:

$$\begin{aligned} \Phi_{out} &= \sum_{i=1}^N \pi \int_{A_i} L_i da_i \\ &= \pi \sum_{i=1}^N \int_{A_i} \sum_{i=0}^3 K_{ji} L_i da_i \\ &= \pi \sum_{i=0}^3 L_i B_i \end{aligned}$$

where:

$$\begin{aligned} A_i &= \int_{A_k} N_i da_k \\ B_i &= \sum_{i=0}^N \int_{A_k} \int_{A_l} N_i \frac{\cos\theta_i \cos\theta_j}{\pi r^2} da_l da_k \end{aligned}$$

Energy conservation requires that:

$$\rho_k \Phi_{in} = \Phi_{out}$$

that is

$$\sum_{i=0}^3 A_i = \sum_{i=0}^3 B_i$$

Consider a special case when only the j th vertex has non-zero luminance. In that case,

$$A_j = B_j \quad \text{for } j = 0, 1, 2, 3.$$

A_i is the area integral of shape function N_i , because:

$$\sum_{i=0}^3 A_i = \text{Area of patch } k$$

This can be written in a form comparable to Eq.(3):

$$\frac{1}{A_i} \sum_{i=0}^N F_{il} = 1$$

where

$$F_{il} = \int_{A_k} \int_{A_l} N_i \frac{\cos\theta_i \cos\theta_j}{\pi r^2} da_l da_k$$

Reciprocity can be written in a form comparable to :

$$F_{il} = F_{jk}$$

where i and j satisfy the condition: $i \text{ mod } 4 = j \text{ mod } 4$. By virtue of this constraint, the shape functions involved in the form factors are the same. Therefore, it is guaranteed that the F_{il} are the same. The physical meaning of this equation is that the fraction of the flux leaving patch k and arriving at patch l equals to the fraction of the flux leaving patch l and arriving at patch k , therefore the system is stable.



3. CALCULATION OF THE NEW FORM FACTOR

In this section, hemisphere projection[3, 4] is used for calculating the form factor of Eq.(5) for an arbitrary convex planar polygon. See Fig.(2) for an example of the hemispherical projection of a triangular patch. The edges of any diffusely-emitting planar polygon which illuminates the point at the center of the hemisphere will intersect the sphere in arcs which are portions of great circles. Those arcs orthogonally project into portions of great ellipses on the equatorial plane of the hemisphere, these portions of great ellipses form an elliptical polygon on the equatorial plane. The area of that elliptical polygon is proportional to the illuminance of the original planar polygon. What we present here is the basis for an algorithm to calculate the illuminance at an arbitrary point P due to the light emitted by a luminous planar triangular patch.

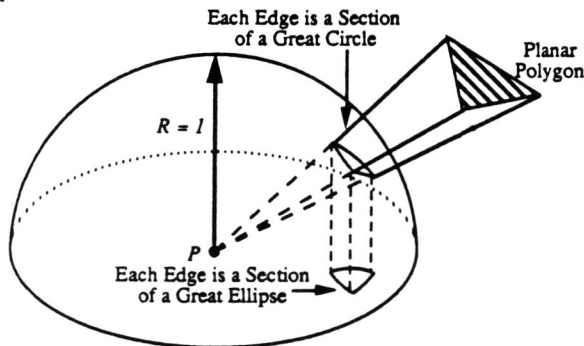


Fig.2 Hemispherical projection of a triangular patch

1) Construct a unit hemisphere with its center at the point P and its equatorial plane tangent to the surface containing P .

2) Project the three vertices of the planar triangle on to the unit hemisphere using lines that pass through the center of the sphere. Given three points: A , B , and C , we have three unit vectors \mathbf{A} , \mathbf{B} , and \mathbf{C} as following:

$$\mathbf{A} = \frac{\overrightarrow{PA}}{|\overrightarrow{PA}|} \quad \mathbf{B} = \frac{\overrightarrow{PB}}{|\overrightarrow{PB}|} \quad \mathbf{C} = \frac{\overrightarrow{PC}}{|\overrightarrow{PC}|}$$

3) Every pair of points lies on a uniquely determined great circle; the intersection of the three great circles form a spherical triangle, which is the spherical projection of the planar triangle. Arbitrarily select two vectors \mathbf{A} and \mathbf{B} . The normal to the great circle containing \mathbf{A} and \mathbf{B} is:

$$\mathbf{N} = -k_1(\mathbf{A} \times \mathbf{B})$$

where k_1 is the normalization factor for \mathbf{N} .

4) The spherical triangle is projected on to the equatorial plane forming a planar elliptical triangle whose edges are arcs of uniquely determined great ellipses. The major axis vector \mathbf{M}_1 and minor axis vector \mathbf{M}_2 are:

$$\mathbf{M}_1 = k_2(\mathbf{Z} \times \mathbf{N})$$

$$\mathbf{M}_2 = \mathbf{Z} \times \mathbf{M}_1 = k_2(\mathbf{Z} \times (\mathbf{Z} \times \mathbf{N}))$$

where k_2 is the normalization factor for \mathbf{M}_1 , and note that $|\mathbf{M}_1| = 1$, $|\mathbf{M}_2| \leq 1$.

5) Using the standard formula for the area of an elliptical sector, the area of the elliptical triangle is computed. This is proportional to the illuminance produced by the planar triangle.

$$F_i = \frac{|\mathbf{M}_2|}{2} \left(a \cos \left(\frac{\mathbf{B} \cdot \mathbf{M}_2}{\mathbf{B} \cdot \mathbf{M}_1} \right) - a \cos \left(\frac{\mathbf{A} \cdot \mathbf{M}_2}{\mathbf{A} \cdot \mathbf{M}_1} \right) \right) \quad (7)$$

And the form factor is now:

$$F = \sum_{i=1}^3 F_i$$

Gaussian quadrature can be applied to the 2-D form factor integral of Eq.(5) when the hemisphere projection has no analytic solution. The Gaussian quadrature method multiplies the function evaluated at a matrix of interpolation points with known weights for each point. The integral is approximated as a summation of these weighted values:

$$\int f(s, t) ds dt = \sum_{i=1}^{N_1} \sum_{j=1}^{N_2} f(s_i, t_j) W_i W_j \quad (8)$$

The accuracy of the approximation depends upon the number of interpolation points, N_1 and N_2 . The differential area of a patch can be expressed as a vector which is the cross product of two vectors lying on the patch

$$d\mathbf{a} = dl_s \times dl_t$$

where

$$dl_s = (x_s \mathbf{x} + y_s \mathbf{y} + z_s \mathbf{z}) ds$$

$$dl_t = (x_t \mathbf{x} + y_t \mathbf{y} + z_t \mathbf{z}) dt$$

with \mathbf{x} , \mathbf{y} , and \mathbf{z} are the unit vectors along x , y , and z axis, x_s and x_t are the partial derivatives of x with respect to s and t , similarly for y_s , y_t , z_s , and z_t . Then with the interpolation method, an arbitrary 3-D planar quadrilateral in xyz space can be transformed to a 2-D square in the st space[11], (see Fig.3), with sides of length of 2:

$$x = \sum_{j=0}^3 N_j x_j \quad y = \sum_{j=0}^3 N_j y_j \quad z = \sum_{j=0}^3 N_j z_j.$$

With $d\sigma = ds dt$, the directional differential can be expressed as:

$$d\mathbf{a} = (S_x \mathbf{x} + S_y \mathbf{y} + S_z \mathbf{z}) d\sigma$$

The form factor K_{ij} can then be computed by Gaussian quadrature:

$$K_{ij} = \int_{\mathbb{R}^2} N_j \frac{(\mathbf{N}_k \cdot \mathbf{r})(\mathbf{N}_l \cdot \mathbf{r})}{\pi r^4} \det |J| d\sigma$$



The form factor K_{ij} can then be computed by Gaussian quadrature:

$$K_{ij} = \int_{\mathbb{R}_{st}} N_j \frac{(N_k \bullet r)(N_l \bullet r)}{\pi r^4} \det|J| d\sigma$$

where r is the vector from vertex i on patch k to the differential area da_l , $\det|J|$ is the determinant of the Jacobian transformation matrix from xyz space to st space. Note here that J is only a 2×2 matrix; since the patch is planar there are only two independent variables among x , y , and z . It is a quantity which includes the weight due to shape functions and the space transformation. The sign of $(N_k \bullet r)$ and $(N_l \bullet r)$ can be used to decide whether or not the illuminating patch k is facing the patch l . By now, the integral has been transformed to the st domain over a 2×2 square, and Eq.(8) can be applied directly for form factor calculation.

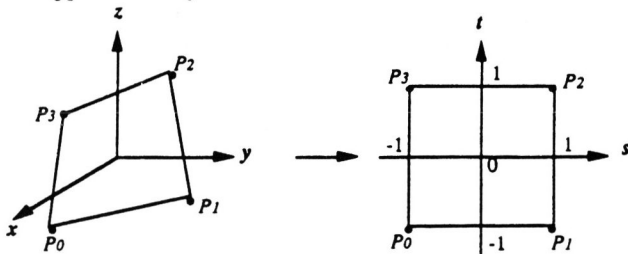


Fig.3 Isoparametric transformation from xyz space to st space

It is useful to describe a situation in which hemispherical projection leads to an analytic solution where numerical solution would not converge. This is the problem raised by considering the luminance on the vertices instead of the center of the patch. Consider the case in which two planar patches, not lying in the same plane, meet along a common edge, i.e., the point P_A on patch A coincides with point P_B on patch B . The luminance at the point P_A due to the patch B will involve all the points on the patch B , including P_B . Since the distance between P_A and P_B is zero, Gaussian quadrature will not give correct result. While in the hemisphere projection, P_A is at the center of the hemisphere, and the patch P_B will be projected on to the hemisphere. Then the form factor can be calculated analytically by the process described in [4].

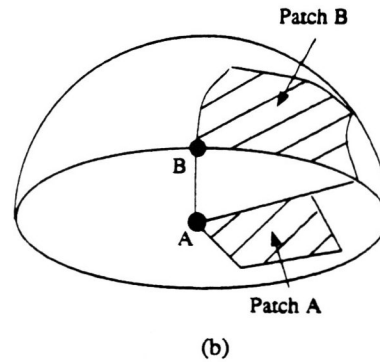
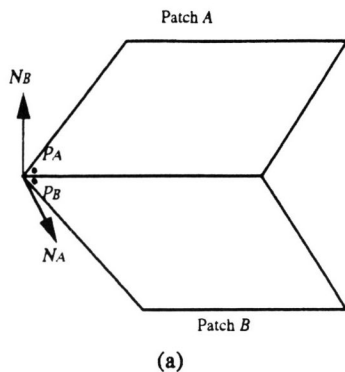


Fig.4 Contribution from close points on a neighboring patch

4. SIMULATIONS, EXPERIMENTS, AND COMPARISONS

Visual assessment, the primary means for judging the realism of images, is inadequate for assessing simulation accuracy because the human eye is not capable of absolute luminance measurement. Our experiments provide a more objective accuracy comparison in the following way. First, images were simulated using the new radiosity model. Then corresponding real scene images were obtained and objective methods for comparing them with simulations were developed. Lastly, the images simulated by uniform luminance and non-uniform luminance assumptions were compared to give a validated measure of the new method.

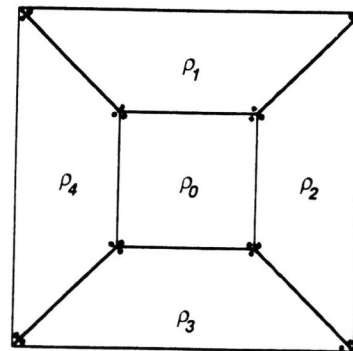


Fig.5 Vertices definition on the surfaces of a box



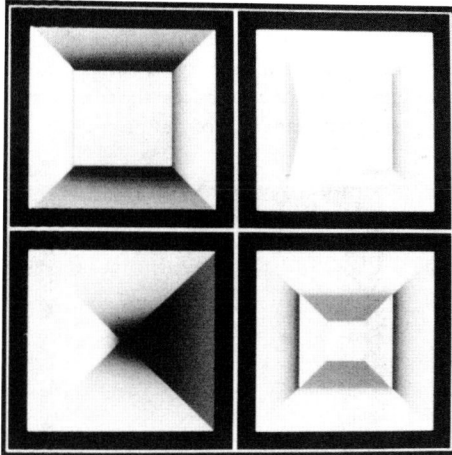


Fig.6 Images generated by new radiosity method

To test the new radiosity model, simulations of images of real objects is necessary. Scenes were simulated out of environments made of boxes and pyramids. The reason for using such simple figures is that we wanted to be able to construct physical replicas that could be compared with synthesized images. The luminances on the internal vertices of patches in the synthesized images were calculated to simulate the real scene luminances. Fig.5 shows the twenty four internal vertices of a box made of materials with diffuse reflectivities ρ_0 through ρ_5 . Note that the front face has been removed and displayed to the right to allow looking inside the box. The simulated images are shown in Fig.6, upper left is a box, upper right is a box with two corners cut, lower left is the cube connected to a pyramid, and lower right is the cube connected to a pyramid with the top of the pyramid cut.

To quantitatively evaluate the simulated images, a simple experimental model (the inside of a box fabricated with diffuse cardboard with various reflectivities) was constructed and photographed. It is impractical to photograph the inside surfaces of a closed box so we used an analogous arrangement. Lights were carefully arranged to produce a uniform illuminance on a diffuse translucent surface with a hole in it. A camera looked through the hole into the open side of the box. All of the box surfaces have different reflectivities. The dimensions and measured reflectivities of the box materials were used in generating the simulated image in Fig.7. The corresponding real digital image produced by this experiment is shown in Fig.8.

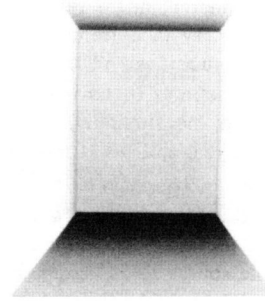


Fig.7 Simulated image of a box

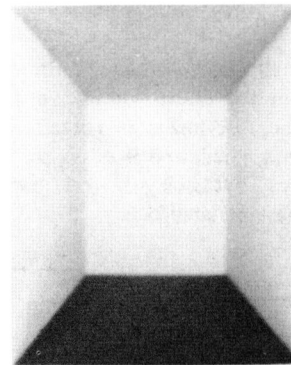


Fig.8 Real image of the box corresponding to Fig.7

Before images can be compared at the pixel level, they must be registered to compensate for the unavoidable differences between the real and simulated imaging conditions. That means that the image gray levels must be normalized and affine transformations must be applied to account for translation and rotation of objects and for perspective errors caused by incorrect lens focal length or camera orientation.

It may be necessary to apply some sort of low-pass filtering, such as Gaussian filtering, to the images to prevent aliasing effects. This is often done when registering images[15]. The generated image was resampled to match the size of the real image to the sub-pixel range and a Mean Square Error Root was computed:

$$MSE(m, n) = \sqrt{\frac{\sum_{i=0}^{N_1} \sum_{j=0}^{N_2} [f_1(i+m, j+n) - \gamma f_2(i, j)]^2}{N_1 N_2}}$$

where m and n were the distances the simulated image was moved in the 2-D pixel space, f_1 and f_2 are the pixel luminances of the simulated and real images, N_1 and N_2 are



image height and width in pixels. Homogeneous transformations were applied to one of the images and the gray level scale factor γ was adjusted until the MSE was minimized. This residual MSE is composed of three components: noise and other errors in the image capture system; round-off and other errors that are inherent in the resampling process; and, simulation inaccuracy. By measurements on the image capture system and by calculations and studies of resampled test images, the first two sources of error have been quantified. The remaining error is the simulation accuracy error. This was computed for the real and simulated images of boxes.

The big luminance difference on the side faces between the real and simulated images can be qualitatively explained as following. The major reason is that in the case of simulation, the distance from the source to the receptor ranges from 0 to 2, while for the real image, the range is from 2 to 4 since the box is open for the light source and the camera. The corresponding luminance ratio by [14] is:

$$\frac{I(0) - I(2)}{I(2) - I(4)} = 36.55$$

Due to the interreflection, the actual ratio will be smaller than this number, but the effect will be very significant. The back face of the real image is not affected much. Then normalization is applied, and it raises the overall luminance of the real image. That is why the real image has much lower contrast than the simulated one.

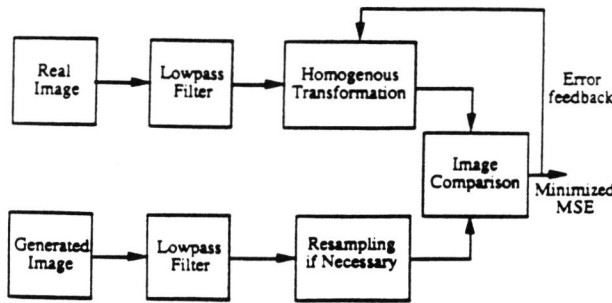


Fig.9 Image registration process

The comparison process is shown in Fig.9. Resampling registers the sizes of the real and simulated images for MSE comparison. Homogeneous transformation places the two images in corresponding positions and orientations. Modification is necessary because the simulation modeled a closed environment but the experimental environment is an open one. Using hemisphere projection techniques this error can be calculated and compensation can be applied, producing a modified simulated image (see Fig.10) with residual MSE of 4.2%. An error image of the real and modified simulation shows that most of the remaining error is due to misalignments along the edges between box surfaces. Some of that error is due to the difficulties in constructing a box to sub-pixel accuracy, so the

measured MSE is probably an upper bound. The actual edge locations could be measured and used as inputs to the simulation if a better estimate is required. Though the comparison methods could be refined further, the current results show that the new radiosity method produces accurate simulations with accuracy near the noise limit of the image capture system.

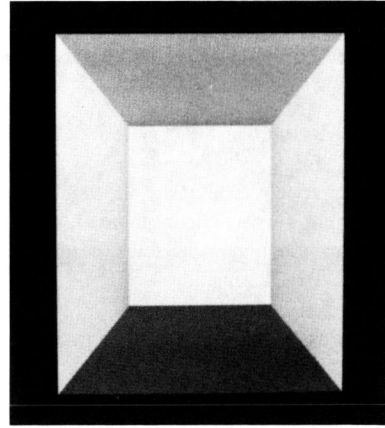
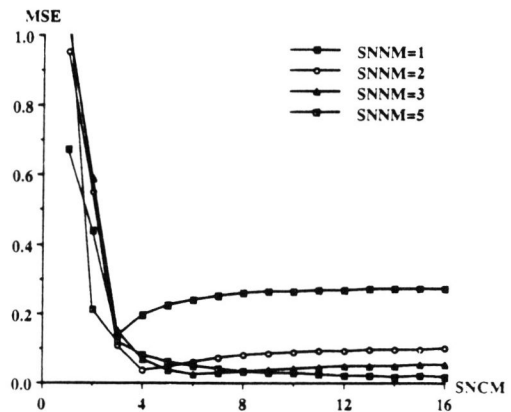


Fig.10 Modified simulation image



(a)

SNNM	1	2	3	4	5	6
SNCM	3	4	6	8	12	16

(b) Best Match List:

Fig.11 Patch number comparison between new and current radiosity methods

Fig.11 shows that the new radiosity method requires fewer patches to produce same accuracy as current radiosity methods. In Fig.11, SNCM means Subdivision Number of Current Method, with each surface divided into $SNCM^2$ patches; SNNM means Subdivision Number of New Method with each surface divided into $SNNM^2$ patches. Fig.11(a) shows the MSE between the images by new method and those



by current methods, Fig.11(b) shows the best match list between SNCM and SNNM. In the worst case, the new approach uses one fourth of number of the patches required by current radiosity methods.

5. CONCLUSIONS

A new radiosity model with non-uniform and continuous patch luminance distribution has been presented. Hemispheric projection was used to calculate the form factor analytically where possible. Otherwise Gaussian quadrature is applied. Images for simple 3-D closed scenes were simulated with the new approach. The corresponding real image from a calibrated imaging system was compared, on a pixel-to-pixel basis, instead of the human visual assessment. MSE measurements were used to evaluate the simulated image and the comparison results are presented which demonstrate that very accurate simulations of a simple environment can be achieved using the model. Images generated by uniform patch luminance radiosity method were compared with the images produced by the non-uniform method, to determine the increase in the number of patches required to achieve a given accuracy using uniform luminance instead of non-uniform luminance, the new radiosity model was proved.

The new radiosity model allows greater flexibility in tessellation and provides accurate interreflection calculations with fewer quadrilateral patches. The quadrilateral tessellation is desirable when curved surfaces are used, tessellation into Bezier patches is most easily accomplished using quadrilateral patches. Also, the new luminance model naturally uses quadrilaterals because of the coordinate transformations that are performed.

Since the luminance distribution is done as part of the interreflection calculation, the interreflection and shading calculations are performed simultaneously. Therefore the consistency of scene luminance simulation and digital image rendering has been kept. This alleviates the need to use an ad hoc interpolation scheme during rendering. Although substantially reduced when compared to previous radiosity methods, Mach band effects remain at common edges where patches meet. This is due to the fact that although the luminances are continuous, the directional derivatives may not be. It appears to therefore be necessary to use higher order approximation to the surface luminance to totally eliminate Mach band effects.

ACKNOWLEDGEMENTS

We would like to acknowledge the support of National Science Foundation under contract No.87008872. Most of this work was performed in the Department of the Electrical Engineering at Worcester Polytechnic Institute. Thanks goes to Gongxian Liu for her help in typing manuscript, to Dr. Matthew Witten for his helpful suggestions and encouragement, to Dr. James Almond for his support.

REFERENCES

- [1] Daniel R. Baum, Stephen Mann, Kevin P. Smith, and James M. Widge. "Making Radiosity Usable: Automatic Preprocessing and Meshing Techniques for the Generation of Accurate Radiosity Solutions," Computer Graphics, (Proc. SIGGRAPH'91), Vol. 25, No. 4, pp.51-60, 1991.
- [2] Daniel R. Baum, Holly E. Rushmeier, and James M. Widge. "Improving Radiosity Solutions Through the Use of Analytically Determined Form-Factors," Computer Graphics, (Proc. SIGGRAPH'89), Vol. 23, No. 3, pp.325-334, 1989.
- [3] Buming Bian. Accurate Simulation of Scene Luminance, Ph. D. Thesis, Worcester Polytechnic Institute, Worcester, MA., June, 1990.
- [4] Buming Bian and Norman Wittels. "Accurate Image Simulation by Hemisphere Projection," Proceedings of SPIE/IS&T, Vol. 1453, San Jose, CA, February, 1991.
- [5] A.T. Campbell, III and Donald S. Fussell. "Adaptive Mesh Generation for Global Diffuse Illumination," Computer Graphics, (Proc. SIGGRAPH'90), Vol. 24, No. 4, pp.155-164, 1990.
- [6] Shenchang Eric Chen. "Incremental Radiosity: An Extension of Progressive Radiosity to an Interactive Image Synthesis System," Computer Graphics, (Proc. SIGGRAPH'90), Vol. 24, No. 4, pp.135-144, 1990.
- [7] Shenchang Eric Chen, Holly E. Rushmeier, Gavin Miller, and Douglass Turner. "A Progressive Multi-Pass Method for Global Illumination," Computer Graphics, (Proc. SIGGRAPH'91), Vol. 25, No. 4, pp.165-174, 1991.
- [8] Michael F. Cohen, Shenchang Eric Chen, John R. Wallace, and Donald P. Greenberg. "A Progressive Refinement Approach to Fast Radiosity Image Generation," Computer Graphics, Vol.22, pp.75-84, 1988.
- [9] Cindy M. Goral, Kenneth E. Torrance, Donald P. Greenberg, and Bennett Battaile. "Modeling the Interaction of Light Diffuse Surfaces," Computer Graphics, Vol.18, pp.213-222, 1984.
- [10] H.C. Hottel and A.F. Sarofim. Radiative Transfer, McGraw-Hill, 1967.
- [11] Thomas J.R. Hughes. The Finite Element Method: Linear Static and Dynamic Finite Element Analysis, Prentice-Hall, Inc., 1987.
- [12] Philip Cooper Magnusson. Development of Methods of Solving Linear Inhomogeneous Equations of the Second Kind Arising in Interreflection and Other Electrical Engineering Field Problems, Ph. D. Thesis, MIT, 1941.
- [13] D.S. Immel Michael F. Cohen, Donald P. Greenberg and P.J. Brock. "An Efficient Radiosity Approach for



- [14] Parry Moon. *The Scientific Basis of Illuminating Engineering*, McGraw-Hill, 1936.
- [15] Harold J. Reitsema, Allen J. Mord, and Eric Ramberg. "High-Fidelity Image Resampling for Remote Sensing," *Proc. SPIE*, Vol.432, pp.211-215, 1983.
- [16] John J. Wallace, Micheal F. Cohen, and Donald P. Greenberg. "A Two Pass Solution to the Rendering Equation: A Synthesis for Ray Tracing and Radiosity Methods," *Computer Graphics*, Vol.21, pp.31-40, 1987.
- [17] Ziro Yamanouti. "Geometrical Calculation of Illumination due to Light from Luminance Sources of Simple Forms," *Res. Electrotech. Lab., Tokyo*, Vol.148, October, 1924.

